Superfluidity at the BEC-BCS crossover in two-dimensional Fermi gases with population and mass imbalance

G. J. Conduit[*]

*Theory of Condensed Matter Group, Department of Physics, Cavendish Laboratory, J. J. Thomson Avenue,
Cambridge, CB3 0HE, United Kingdom*

P. H. Conlon

Rudolf Peierls Centre for Theoretical Physics, 1 Keble Road, Oxford, OX1 3NP, United Kingdom

B. D. Simons

*Theory of Condensed Matter Group, Department of Physics, Cavendish Laboratory, J. J. Thomson Avenue,
Cambridge, CB3 0HE, United Kingdom*

We explore the zero-temperature phase behavior of a two-dimensional two-component atomic Fermi gas with population and mass imbalance in the regime of the BEC-BCS crossover. Working in the mean-field approximation, we show that the normal and homogeneous balanced superfluid phases are separated by an inhomogeneous superfluid phase of Fulde-Ferrel-Larkin-Ovchinnikov (FFLO) type. We obtain an analytical expression for the line of continuous transitions separating the normal and inhomogeneous FFLO phases. We further show that the transition from the FFLO phase to the homogeneous balanced superfluid is discontinuous leading to phase separation. If the species have different masses, the superfluid phase is favored when the lighter species is in excess. We explore the implications of these findings for the properties of the two-component Fermi gas in the atomic trap geometry. Finally, we compare and contrast our findings with the predicted phase behavior of the electron-hole bilayer system.

I. INTRODUCTION

By controlling interaction through a magnetically tuned Feshbach resonance, ultracold atomic Fermi gases have provided a versatile arena in which to explore pairing phenomena and superfluidity [1–3]. Already the crossover between the Bose-Einstein condensate (BEC) phase of strongly bound diatomic molecules to the BCS phase of weakly bound Cooper pairs has been observed experimentally [1,4–8]. In recent years, much attention has been focused on the phase behavior of two-component Fermi gases with population imbalance [9–27], and generalized mass ratios between different species [25,28–35]. The symmetry breaking effect of population and mass imbalance destabilizes the condensate leading to an enriched phase diagram characterized by tricritical point behavior with first-order transitions separating normal and superfluid phases at low temperatures [36]. More detailed studies have shown that, on the weak coupling side of the crossover, the transition into a homogeneous superfluid phase at low temperatures is preempted by the development of an inhomogeneous superfluid phase [9,14,18,37–43]. This is a manifestation of the Fulde-Ferrel-Larkin-Ovchinnikov (FFLO) phase predicted to occur in superconducting electron systems subject to a Zeeman field [44,45]. In the three-dimensional system, the FFLO phase is predicted to occupy only a small region of the phase diagram making its experimental identification in the atomic trap geometry challenging. Indeed, even in solid state systems, the FFLO phase has only recently been observed [46].

The potential for an FFLO instability at a single wave vector in a three-dimensional ultracold atomic gas with only population imbalance was explored by Refs. [17] and [24]. They found a stable FFLO phase only on the BCS side of the resonance. Additionally Ref. [47] showed the three-dimensional system is unstable to FFLO superfluid currents, but these were not found in the nonuniform three-dimensional trap experiments of Ref. [48].

Lately, efforts have been made to explore the effects of population imbalance on pairing in two-component Fermi gases in two-dimensions. Although the phase diagram of the zero-temperature system has been explored in the regime of BEC-BCS crossover in the mean-field approximation [23], the potential for FFLO phase formation has not yet been addressed. By contrast, motivated by potential applications to strongly anisotropic layered systems, several theoretical studies have explored the potential for superconducting FFLO phase formation in two-dimensional electron systems [49–51]. A quasiclassical analysis by Ref. [52], involving a Ginzburg-Landau expansion of the free energy in Fourier components of the superconducting order parameter, found that the FFLO transition in two dimensions was continuous at low temperatures. In a separate study of condensation in electron-hole bilayers [50], it was argued that the FFLO phase can occupy a significant part of the two-dimensional phase diagram. Motivated by these investigations, and the potential impact on the atomic gas system, in the following we will investigate the potential for FFLO phase formation in the two-dimensional two-component Fermi gas addressing both population imbalance and generalized mass ratios.

In the context of ultracold atomic Fermi gases, a two-dimensional system can be experimentally realized by con-

---

*gjc29@cam.ac.uk

fining the gas with a one-dimensional optical lattice consisting of two counterpropagating laser beams [53–56]. These impose a periodic potential, with antinodes spaced every half wavelength. The interwell barrier energy, and therefore the tunneling rate, depends on the laser intensity, which should be chosen to be much higher than the species chemical potential and the superfluid gap [57,58]. This inhibits transfer of atoms between layers and the Fermi gas separates into stacked quasi-two-dimensional layers. The depth of the optical potential can always be varied independently of the external harmonic trapping potential and species chemical potentials so it should always be possible to reduce the tunneling rate sufficiently that the cold atom gas can be regarded as being two-dimensional. Within a layer, the short-ranged interaction of the atoms can be adjusted by exploiting a Feshbach resonance. It has been suggested [59] that due to the possible formation of dressed molecules a single band theory could incorrectly predict cloud size in the strong-coupling limit. However, here we are interested in the weak-coupling limit and the behavior at the BEC-BCS crossover where we believe that a single-band theory will encompass the essential behavior allowing us to capture the qualitative phase structure.

Finally, further motivation for the investigation of superfluidity in the mass imbalanced system comes from studies of exciton condensation in bilayer electron-hole systems. In recent years, attempts to realize a condensed exciton phase have focused on quantum well structures where electrons and holes are restricted to neighboring two-dimensional layers [49–51]. The range of the Coulomb interaction between the particles can be shortened by introducing a screening layer. As with the two-component Fermi gas, the electron-hole system affords the possibility of tuning between a superfluid of tightly bound pairs (excitons) to a condensate phase of an electron-hole plasma. Moreover, while one can, in principle, engineer a balanced electron-hole population, the effective masses of the electron and hole quasiparticles in the semiconductor are typically quite different. In GaAs, the ratio of the hole to electron mass is around $m_h/m_e=4.3$. Condensation phenomena in mass imbalanced systems have also been explored in the context of quantum chromodynamics, where the particles represent different species of quarks [60].

The remainder of the paper is organized as follows. In Sec. II we begin by deriving an expression for the thermodynamic potential in the mean-field approximation for the two-component Fermi gas allowing for the development of an inhomogeneous condensate phase. In Sec. III we use this result to elucidate the zero-temperature phase diagram of the system for a uniform order parameter both at fixed chemical potential and fixed number density. In Sec. IV we explore the tendency of the system to condense into an inhomogeneous superfluid phase. In particular we combine the results of a Ginzburg-Landau expansion with the numerical analysis of the thermodynamic potential to infer the region over which the inhomogeneous phase persists. Finally, in Sec. V, we examine the properties of the atomic Fermi gas in the harmonic trap geometry, concluding our discussion in Sec. VI.

II. MEAN-FIELD THEORY

Our starting point is a two-component Fermi gas with each species indexed by a pseudospin $\sigma \in \{\uparrow,\downarrow\} \equiv \{+1,-1\}$.

The single-particle dispersion $\epsilon_{\mathbf{k},\sigma}=k^2/2m_\sigma$ depends on the different effective masses of the two species m_σ, throughout we set $\hbar=1$. Introducing the reduced mass $1/m_R=(1/m_\uparrow +1/m_\downarrow)/2$ and the mass ratio $r=m_\downarrow/m_\uparrow$ we have $m_\uparrow=m_R(1 +1/r)/2$ and $m_\downarrow=m_R(1+r)/2$. To enforce a population imbalance, each species must be associated with its own chemical potential $\mu_\sigma=\mu+\sigma h$. With these definitions, one may see that the phase diagram of the system is symmetric under the transformation $(h,r)\mapsto(-h,1/r)$.

In the following, we will focus on the zero-temperature phase behavior of the system as predicted by mean-field theory. In doing so, we will miss nonperturbative effects that appear at large mass ratios. In particular, when the ratio of masses is greater than 13.6, it is known that, in three-dimensions, two heavy and one light fermion can form a three-body weakly bound state [61–63]. Our analysis does not include the possibility of such a state.

To explore the regime of BEC-BCS crossover, we will focus our attention on a single-channel Hamiltonian describing a wide Feshbach resonance where the closed channel population remains small throughout [24,64,65]. The quantum partition function for the system can then be expressed as a functional field integral over fermionic fields ψ_σ and $\bar{\psi}_\sigma$, $\mathcal{Z}=\int e^{-S[\bar{\psi},\psi]}\mathcal{D}\psi\mathcal{D}\bar{\psi}$, with the action

$$S[\psi,\bar{\psi}]=\int_0^\beta d\tau\left[\sum_{\mathbf{k},\sigma}\bar{\psi}_{\mathbf{k},\sigma}(\partial_\tau+\xi_{\mathbf{k},\sigma})\psi_{\mathbf{k},\sigma}\right.$$
$$\left.-\frac{1}{2}\sum_{\mathbf{k},\mathbf{k}',\mathbf{q}}\bar{\psi}_{\mathbf{k},\uparrow}\bar{\psi}_{\mathbf{q}-\mathbf{k},\downarrow}V_{\mathbf{k}'-\mathbf{k}}\psi_{\mathbf{k}',\downarrow}\psi_{\mathbf{q}-\mathbf{k}',\uparrow}\right],$$

where V denotes the two-body interaction potential and $\beta =1/k_BT$ is the inverse temperature. Here, for brevity, we have set $\xi_{\mathbf{k},\sigma}=\epsilon_{\mathbf{k},\sigma}-\mu_\sigma$. Anticipating the development of pair correlations, we introduce a Hubbard-Stratonovich decoupling of the interaction in the Cooper channel, with $\mathcal{Z} =\int e^{-S[\psi,\bar{\psi},\Delta,\bar{\Delta}]}\mathcal{D}\psi\mathcal{D}\bar{\psi}\mathcal{D}\Delta\mathcal{D}\bar{\Delta}$, where the action now takes the form

$$S[\psi,\bar{\psi},\Delta,\bar{\Delta}]=\sum_{\omega,\mathbf{k},\mathbf{k}'}\bar{\Delta}_{\omega,\mathbf{k}}(V^{-1})_{\mathbf{k}'-\mathbf{k}}\Delta_{\omega,\mathbf{k}'}$$
$$+\sum_{\omega,\mathbf{k},\mathbf{q}}(\bar{\psi}_{\omega,\mathbf{q}/2-\mathbf{k},\uparrow}\quad\psi_{\omega,\mathbf{q}/2+\mathbf{k},\downarrow})$$
$$\times\begin{pmatrix}-i\omega+\xi_{\mathbf{k}-\mathbf{q}/2,\uparrow} & \Delta_{0,\mathbf{q}}\\ \bar{\Delta}_{0,\mathbf{q}} & -i\omega-\xi_{\mathbf{k}+\mathbf{q}/2,\downarrow}\end{pmatrix}$$
$$\times\begin{pmatrix}\psi_{\omega,\mathbf{q}/2-\mathbf{k},\uparrow}\\ \bar{\psi}_{\omega,\mathbf{q}/2+\mathbf{k},\downarrow}\end{pmatrix}.$$

Anticipating that the transition to the superfluid (SF) from the normal phase is continuous (a property already established in the weak-coupling limit of the two-dimensional system by Ref. [52]), we will suppose that the order parameter is characterized by a single plane-wave state corresponding to the stationary saddle-point solution $\Delta_{\omega,\mathbf{q}}=\Delta_{\mathbf{Q}}\delta_{\mathbf{q},\mathbf{Q}}\delta_{\omega,0}$ [17,24,66]. In this case, $\mathbf{Q}=0$ describes the homogeneous SF state while, for $\mathbf{Q}\neq0$, the condensate is of FFLO type. If the

transition to the inhomogeneous phase is first order, the single wave vector assumption necessitates some degree of approximation that will underestimate the width of the FFLO region in the phase diagram.

Then, approximating the functional integral over fields Δ by its mean-field value, and taking the interaction to be contact, $V(\mathbf{r}) = g\delta^2(\mathbf{r})$, integration over the fermionic fields gives the thermodynamic potential

$$\Omega = \frac{|\Delta_{\mathbf{Q}}|^2}{g} + \sum_{\mathbf{k}} (\xi_{k,+} - \overbrace{E_{\mathbf{k}}}^{\ddagger}) - \frac{1}{\beta}\text{Tr}\ln(1 + e^{-\beta(E_{\mathbf{k}}+\sigma\xi_{\mathbf{k},-})}), \tag{1}$$

where $\xi_{\mathbf{k},\pm} = (\xi_{\mathbf{k}-\mathbf{Q}/2,\uparrow} \pm \xi_{\mathbf{k}+\mathbf{Q}/2,\downarrow})/2$ and $E_{\mathbf{k}} = (\xi_{\mathbf{k},+}^2 + |\Delta_{\mathbf{Q}}|^2)^{1/2}$. From this expression, one can obtain the polarization or "magnetization"

$$m \equiv n_\uparrow - n_\downarrow = -d\Omega/dh = n_F(E_{\mathbf{k}} - \xi_{\mathbf{k},-}) - n_F(E_{\mathbf{k}} + \xi_{\mathbf{k},-}), \tag{2}$$

and the total number density

$$\begin{aligned} n &\equiv n_\uparrow + n_\downarrow \\ &= -d\Omega/d\mu \\ &= 1 + \frac{\xi_{\mathbf{k},+}}{E_{\mathbf{k}}}[n_F(E_{\mathbf{k}} - \xi_{\mathbf{k},-}) + n_F(E_{\mathbf{k}} + \xi_{\mathbf{k},-}) - 1], \end{aligned} \tag{3}$$

where $n_F(E) = 1/(1 + e^{-\beta E})$ denotes the Fermi function.

Finally, to regularize the unphysical UV divergences associated with the δ-function form of contact interaction [and contained within the term labeled by $\ddagger$ in Eq. (1)], we will set

$$\frac{1}{g} = \int_0^\infty \frac{1}{2E + E_b}dE, \tag{4}$$

where E_b denotes the energy of the two-body bound state [23,67]. E_b will then be used as a control parameter to tune through the BEC-BCS crossover. As E_b is increased, the system evolves continuously from the weak coupling BCS phase to the strong-coupling BEC phase of tightly-bound pairs.

Having obtained the thermodynamic potential in the mean-field approximation, we now outline our strategy for calculating the zero-temperature phase diagram. As a platform to address the potential for inhomogeneous phase formation, in the following section we begin by establishing the phase diagram associated with a uniform order parameter, i.e., $\mathbf{Q}=\mathbf{0}$. In this case, the integrations associated with the thermodynamic potential (1) can be evaluated analytically and many key features of the generalized phase diagram understood. Then, in Sec. IV, we return to the more general situation, exploring the capacity for inhomogeneous phase formation. After confirming that, in the single wave vector approximation, the transition to the SF phase is always continuous, we develop a Ginzburg-Landau expansion of the action to determine the locus of the normal-FFLO phase boundary analytically. Combining these results, we determine the phase diagram for a spatially uniform system as a function of fixed chemical potential and, separately, as a function of fixed particle number. Finally, in Sec. V, we apply these results to the problem of resonance superfluidity in the physically realizable harmonically trapped system.

III. UNIFORM SUPERFLUID

In this section we focus on the phase diagram of a system in which the order parameter is constrained to be uniform. At zero temperature, setting $\mathbf{Q}=\mathbf{0}$, the thermodynamic potential can be evaluated analytically for arbitrary population imbalance and mass ratio

$$\begin{aligned} \frac{2\Omega}{\nu} &= |\Delta_0|^2\left[\ln\left(\frac{\sqrt{\mu^2+|\Delta_0|^2}-\mu}{E_b}\right) - \frac{1}{2}\right] - \mu(\sqrt{\mu^2+|\Delta_0|^2}+\mu) - \theta(h'^2 - |\Delta_0|^2)\left\{\theta(\mu_f - Rh' - \mu_c)\left(2|h'|\mu_c - |\Delta_0|^2\ln\left|\frac{\mu_c + |h'|}{\mu_c - |h'|}\right|\right)\right. \\ &\quad + \theta(\mu_c + \mu_f - Rh')\theta(\mu_c - \mu_f + Rh')\left[|h'|(\mu_c + 2\mu_f) - \mu\sqrt{\mu^2+|\Delta_0|^2} - |\Delta_0|^2\ln\left|\frac{\mu_c + |h'|}{\sqrt{\mu^2+|\Delta_0|^2}-\mu}\right|\right. \\ &\quad \left.\left. + \text{sgn}(h')\left(R(\mu^2 - h'^2) + \frac{|\Delta_0|^2}{2}\ln(r)\right)\right]\right\}. \end{aligned} \tag{5}$$

Here θ denotes the Heaviside step function, $\nu = m_R/2\pi$ the two-dimensional density of states of the reduced mass system and, for clarity, we have defined the set of parameters

$$R \equiv \frac{r-1}{r+1}, \quad h' \equiv \frac{h - \mu R}{\sqrt{1-R^2}}, \quad \mu_c \equiv \sqrt{h'^2 - |\Delta_0|^2},$$

$$\mu_f \equiv \mu\sqrt{1-R^2}. \tag{6}$$

By minimizing the thermodynamic potential with respect to Δ_0, one obtains the loci of phase boundaries shown in Table I. When the mass ratio is unity ($R=0$), these results coincide with those obtained in Ref. [23]. In particular, one may note that, in the SF phase, the order parameter takes the form

TABLE I. Summary detailing the loci of phase boundaries for μ/E_b as a function of h/E_b and $R=(r-1)/(r+1)$. Results labeled with an asterisk are found in and are relevant for Sec. IV.

PP-FFLO*	$[1+(h/E_b)R \pm \sqrt{1+2(h/E_b)R-R^2-2(h/E_b)R^3}]/R^2$
FFLO-SF* and PP-SF	$\{1+2(h/E_b)R-R^2-\sqrt{(1-R^2)[1+4(h/E_b)R]}\}/2R^2$
FP-SF	$[\sqrt{2}(h/E_b)+\sqrt{1-R}]/(\sqrt{2}-2\sqrt{1-R})$
ZP-FP	$\pm(h/E_b)$
FP-FFLO* and FP-PP	$\mp(h/E_b)$
ZP-SF	$-1/2$

$$|\Delta_0| = \sqrt{E_b(2\mu+E_b)},$$

implying a thermodynamic potential $\Omega=-\nu(\mu+E_b/2)^2$, independent of the chemical potential difference h. As a result, one may infer that the magnetization $m=-d\Omega/dh$ is zero. For the uniform condensate, the SF phase always involves a balanced population of fermions. Drawing on these results, let us now comment on the implications for the phase diagram of the system for, respectively, fixed chemical potential and fixed particle number.

A. Fixed chemical potentials

When the chemical potentials μ and h are held constant, minimization of the thermodynamic potential leads to the phase diagram depicted in Fig. 1. The equal mass case is consistent with the result of Ref. [23]. For μ smaller than either the molecular binding energy per particle $-E_b/2$, or the chemical potential shift associated with the majority species $-h$ (corresponding to an empty Fermi surface), the equilibrium phase hosts no particles (the "zero-particle" state, ZP). On increasing the chemical potential μ a second-order phase transition into either a balanced SF, or a fully polarized (FP) normal phase occurs. The transitions from the zero particle phase to a FP normal phase, and from a FP phase to a
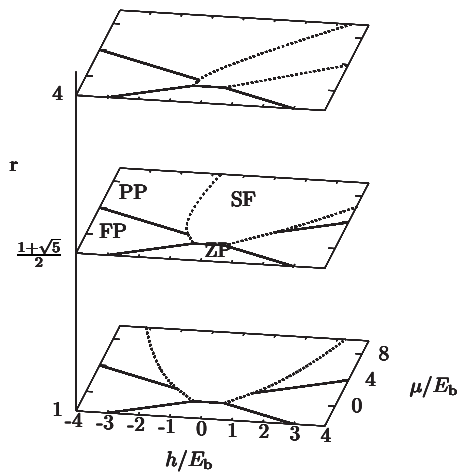

FIG. 1. The phase diagram shown as a function of $(h/E_b,\mu/E_b)$ for three different values of the mass ratio r. The diagrams were constructed assuming a uniform order parameter, neglecting the potential for inhomogeneous phase formation. The solid lines represent continuous phase boundaries, while the dashed lines denote first-order transitions into the balanced SF phase.

partially polarized (PP) normal phase are both continuous. The phases have boundaries where the Fermi surface shrinks to zero at $\mu=-h$ and $\mu=+h$, respectively (for $h>0$). At fixed E_b, an increase in chemical potential μ leads to an increase in the order parameter of the balanced superfluid system $|\Delta_0| \propto \sqrt{\mu}$ and an attendant increase in the critical h required to destroy the condensate. The phase transition from the normal state, both FP and PP, into the SF is first order.

As the ratio of masses is increased, as shown in Fig. 1 on the side $r>1$, the phase diagram becomes skewed. This can be understood by tracking the locus of the line where the Fermi surfaces of the two species are perfectly matched, approximately along the center of the SF phase. The central superfluid locus is $\mu/h=1/R$, which is consistent with the skew. Superfluidity is therefore more favorable if the "light" species has a greater chemical potential than the "heavy" species.

B. Fixed number densities

In the canonical ensemble, where the number densities n and m are held constant, the chemical potentials μ and h must be inferred self-consistently. In this case, a first-order transition in the $(\mu/E_b,h/E_b)$ phase diagram (Fig. 1) implies phase separation (PS) [9] in the (n,m) phase diagram. At each point along the PP-SF phase boundary in $(\mu/E_b,h/E_b)$ one can evaluate the corresponding polarization and total number density. From this result, one can infer the boundaries between the normal and phase separated regions as functions of E_b/E_F and polarization m/n. Here we have defined a "Fermi energy" scale $E_F=n/v$, where $v=m_R/2\pi$ denotes the constant two-dimensional density of states of the reduced mass system. The resulting phase diagram is shown in Fig. 2.

As expected, in the BEC limit of large E_b/E_F, one finds phase separation, with the development of a condensate of tightly bound molecular pairs coexisting with a FP phase containing excess fermions. The phase diagram shows that this behavior persists into the weak-coupling BCS limit, with the system phase separating into a balanced SF phase (i.e., with $m/n=0$), and the excess particles forming a noninteracting PP Fermi gas. In the BCS limit of weak pairing, a small population imbalance is sufficient to destroy pairing and enter the PP normal phase region.

When the species have unequal masses, the phase diagram is skewed, similar to the fixed chemical potential case in Sec. III A. If there is a mass imbalance then the Fermi energy of each spin species scales as $E_{F,\sigma}=n_\sigma/v_\sigma \equiv \pi(n$
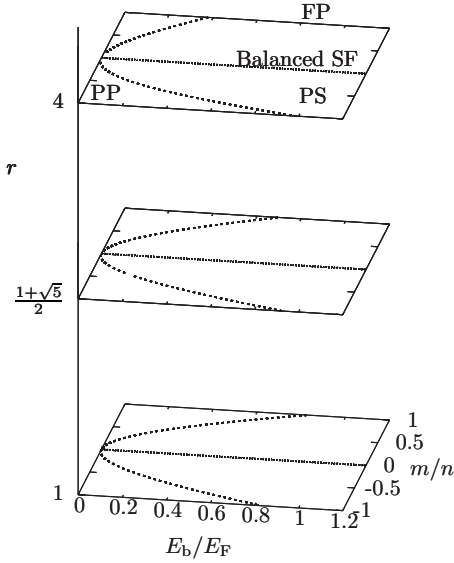
FIG. 2. The phase diagram as a function of m/n and interaction strength E_b/E_F of the two-dimensional system with fixed majority and minority particle densities for three different mass ratios r. The SF phase (dotted line) is the line of zero population imbalance. Between the balanced SF and PP/FP phase (dashed line) lies a region of phase separation (PS).

$+\sigma m)/m_\sigma \propto 1/m_\sigma$ implying that it is energetically more beneficial for the "heavy" rather than "light" particles to be in the normal state. Therefore, at a given mass imbalance, the phase diagram loses its symmetry in m/n and superfluidity is favored if the "lighter" species is in excess whereas the normal state is favored if the "heavy" species is in excess.

IV. INHOMOGENEOUS SUPERFLUID

With the properties of the uniform SF phase in place, we now turn to the question of inhomogeneous phase formation. To characterize the nature of the PP-FFLO transition, we adopt two methodologies: first, in Sec. IV A, we will develop a Ginzburg-Landau expansion of the action to explore the locus of putative continuous transitions from the normal PP phase into the inhomogeneous FFLO phase. Second, in Sec. IV B, we will assess the validity of the Ginzburg-Landau expansion by investigating the global minimum of the thermodynamic potential for a mean-field order parameter field involving a single wave vector. Using these results, we will infer the phase diagram of a system with fixed chemical potentials in Sec. IV C and fixed particle densities in Sec. IV D.

A. Ginzburg-Landau theory

With the ansatz that the transition from the normal to condensed phase is continuous, close to the transition we may expand the action in fluctuations $|\Delta_{\mathbf{q}}|$. In doing so, one obtains

$$S_{\text{eff}} = \sum_{\mathbf{q}} \alpha_{\mathbf{q}} |\Delta_{\mathbf{q}}|^2 + O(|\Delta|^4), \tag{7}$$

where

$$\alpha_{\mathbf{q}} = \sum_{\mathbf{k}} \left(\frac{1}{2\epsilon_{\mathbf{k}} + E_b} - \frac{1 - n(\xi_{\mathbf{k}-\mathbf{q}/2,\uparrow}) - n(\xi_{\mathbf{k}+\mathbf{q}/2,\downarrow})}{\xi_{\mathbf{k}-\mathbf{q}/2,\uparrow} + \xi_{\mathbf{k}+\mathbf{q}/2,\downarrow}} \right)$$

denotes the static pair susceptibility. The locus of continuous transitions may be determined from the value of $\mathbf{q}$ at which $\alpha_{\mathbf{q}}$ is both minimized and passes through zero. Within the condensed phase, higher-order terms in $\Delta_{\mathbf{q}}$ determine the crystalline structure of the FFLO state [68].

The corresponding phase boundary then translates to the largest allowable chemical potential shift h which occurs when the Fermi surfaces just touch but do not cross [52]. From this condition, one finds a phase boundary along the line

$$\frac{h}{E_b} = \left(\frac{\mu}{E_b} - 1 \right) R \pm \sqrt{\left(\frac{2\mu}{E_b} - 1 \right)(1 - R^2)}. \tag{8}$$

Minimizing $\alpha_{\mathbf{q}}$ with respect to $|\mathbf{q}|$, one obtains the further condition $\epsilon_{\mathbf{q}} \equiv q^2/(2m_R) = 2E_b/(1-R^2)$. Measured in units of the Fermi momentum of the reduced mass system, this translates to a wave vector

$$\frac{|\mathbf{q}|}{k_F} = \sqrt{\frac{E_b}{E_F} \frac{(m_\uparrow + m_\downarrow)}{2m_R}}, \tag{9}$$

where $k_F^2 = 2m_R E_F$ and, inverting Eq. (8), $E_b = \mu - hR \pm \sqrt{(\mu^2 - h^2)(1-R^2)}$. In the weak-coupling limit $E_b \ll E_F$, so that at equal masses $E_b = h^2/2\mu$ giving $|\mathbf{q}| = 2h/v_F$, where v_F is the Fermi velocity, agreeing with the findings of Burkhardt and Rainer [69], Shimahara [70], and Combescot and Mora [52]. In the same limit, the pair susceptibility takes the form $\text{Re}\{\ln[1 + \sqrt{1 - (|\mathbf{q}| v_F/2h)^2}]\}$, collapsing to that found in previous works.

B. FFLO instability phase boundaries

To assess whether the transition from the PP phase to the FFLO phase is really continuous, one can instead minimize the thermodynamic potential Eq. (1) with respect to the wave vector $\mathbf{Q}$ and the mean-field value of the order parameter $\Delta_{\mathbf{Q}}$. For several values of chemical potential μ and two different mass ratios $r=1$ and $r=2$, numerical minimization of the thermodynamic potential confirms that the order parameter changes continuously, falling to zero along a line of instability (see Fig. 3). The locus of the transition also agrees with that obtained from the Ginzburg-Landau expansion in Sec. IV A. This result is in accord with that found in Ref. [52] in the weak-coupling limit of the equal mass system, and shows that the transition remains continuous across the entire range of the FFLO phase.

We are now in a position to evaluate all phase boundaries associated with the FFLO instability. The agreement described above between Ginzburg-Landau theory and direct minimization allows us to use the analytic Ginzburg-Landau boundary between the PP and FFLO phases. The minimum in the thermodynamic potential that gives rise to the FFLO phase is shallow relative to that of the SF phase. We are therefore able to approximate the actual FFLO-SF phase boundary by the $\mathbf{Q}=0$ result for the PP-SF boundary described in Sec. III. A summary of the phase boundaries is
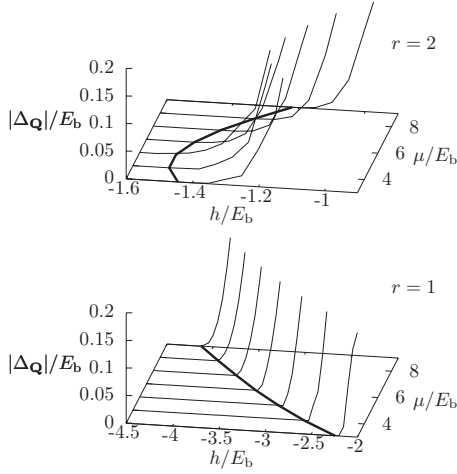
FIG. 3. Variation of the order parameter $|\Delta_{\mathbf{Q}}|/E_b$ with chemical potential difference h/E_b and chemical potential μ/E_b. The upper panel is at a mass ratio $r=2$, and the lower panel at equal masses, $r=1$. The thin black lines trace out the $|\Delta_{\mathbf{Q}}|/E_b$ variation, found by minimizing the thermodynamic potential (1), for several different chemical potentials. The thick black line is the locus of the second-order transition predicted by Ginzburg-Landau theory.

shown in Table I, the additional boundaries due to the presence of the FFLO phase are labeled with an asterisk. As the extent of the SF region is only reduced by the presence of the FFLO phase, the SF is balanced, as was shown for the $\mathbf{Q}=0$ study in Sec. III.

C. Fixed chemical potentials

Let us now apply these results to the problem of a uniform system with constant chemical potentials. The corresponding phase diagram is shown in Fig. 4. While the general topology of the phase diagram mirrors that discussed in Sec. III A, the transition to the balanced SF phase is preempted by the formation of an inhomogeneous FFLO phase. The FFLO instability occurs mainly on the PP side of the PP-SF phase boundary of the uniform condensate shown in Fig. 1 with just a small intrusion on the balanced SF side. The FFLO instability does not occur within the FP state as there are no minority state particles with which to pair. The FFLO-PP boundary is second order, while the FFLO-SF boundary is first order.

The FFLO-PP phase boundary terminates at the SF phase for small mass ratios and at the FP phase for large mass ratios on the side of the majority "heavy" species. The movement of the boundary terminus with increasing mass ratio r is in the opposite direction on the majority "light" species side—it moves further up the SF phase boundary. The special mass ratio where it terminates at the SF-FP phase boundary on the majority "heavy" species side is at $r_c = (1+\sqrt{5})/2$.

The thermodynamic potential variation is also shown in Fig. 4 at four different points (a), (b), (c), (d) for $r=1$. Since the wave vector dependence of the thermodynamic potential enters through the order parameter, in both the PP (a) and FP (d) normal phases the minimum is $|\mathbf{Q}|$ independent. At the highlighted FFLO phase point (b), the global minimum lies at $|\Delta_{\mathbf{Q}}| \approx 0.2E_b$ with $|\mathbf{Q}| \approx 2\sqrt{m_R E_b}$, while a local minimum also develops at $|\Delta_{\mathbf{Q}}| \approx 3.8E_b$ with $|\mathbf{Q}|=0$ corresponding to the putative uniform SF phase. At the highlighted SF point (c), the global minimum lies at $|\Delta_{\mathbf{Q}}| \approx 3.8E_b$ and $|\mathbf{Q}|=0$.

D. Fixed number densities

Let us now address the implications of the phase diagram for a spatially uniform system held at fixed number densities.
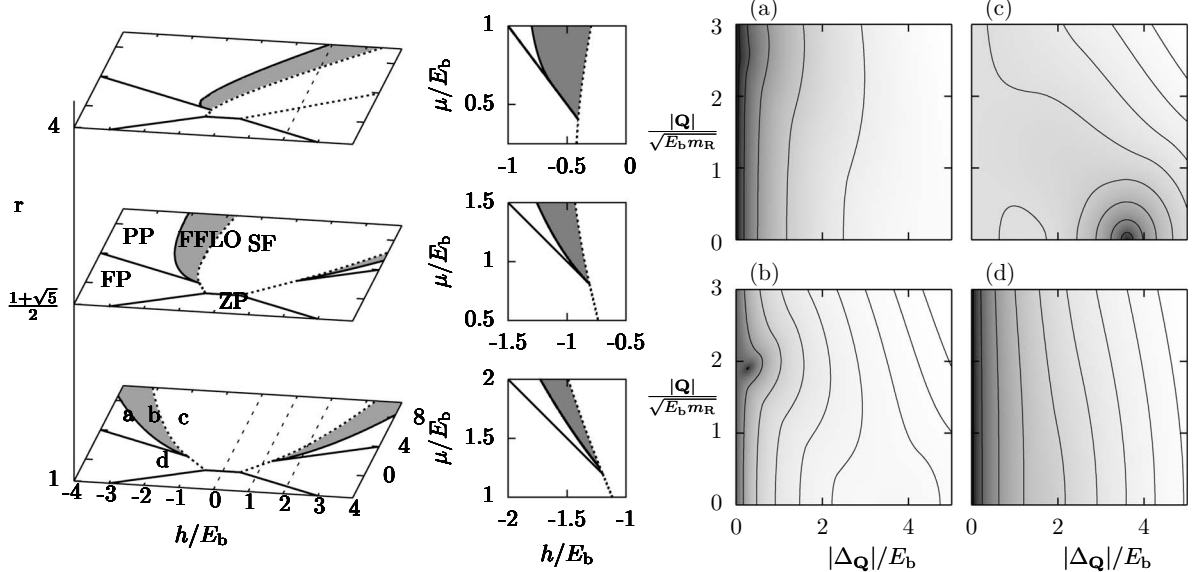

FIG. 4. The left-hand column shows the phase diagram in $(\mu/E_b, h/E_b)$ at three different mass ratios r. The solid lines represent second-order phase boundaries, the dashed line denotes first-order phase transitions into the balanced SF phase. The FFLO phase is highlighted in gray. The trajectories followed in the sample traps in Sec. V are shown by thin dashed lines. The central column of diagrams focus more closely on the topology of the phase diagram close to the tricritical point region for $h/E_b < 0$. Thermodynamic potential surfaces are shown in the right-hand column; the darker the more negative and so more favorable; label (a) is a PP normal state, (b) a FFLO state, (c) a SF state, and (d) a FP state. Different plots have different shading calibrations, (unequally spaced) contour lines are also shown.
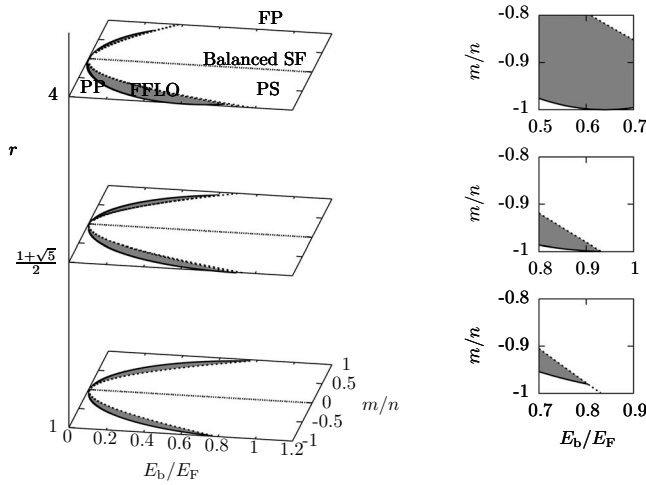
FIG. 5. The phase diagram in $(m/n, E_b/E_F)$ of the two-dimensional system with fixed majority and minority particle densities for three different mass ratios r. The SF phase (dotted line) is represented by the line of zero population imbalance $m/n=0$. The PP phase is separated from the FFLO phase (highlighted in gray) by a second-order phase boundary (solid line). In the phase separated (PS) region bordered by the dashed line, the system separates into a balanced superfluid (SF) and either a normal phase or, depending on the composition, an inhomogeneous FFLO phase. The right-hand column of graphs focus on the terminus of the PP-FFLO phase boundary on the side of negative polarization for the three featured mass ratios.

Obtaining the corresponding density n and magnetization m gives the phase diagram shown in Fig. 5. Once again, the topology of the phase diagram mirrors that discussed for the homogeneous condensate in Sec. III B. However, between the phase separated SF phase and normal phase, the system exhibits an inhomogeneous FFLO phase over a wide region of the phase diagram.

In the weak-coupling BCS limit, even a small population imbalance is sufficient to enter the FFLO phase region. We note that in a population balanced system the Fermi momenta of the populations are equal so no shift of the Fermi surfaces is required to form Cooper pairs and a modulated phase is not seen.

The effects of the moving PP-FFLO phase boundary terminus, described in Sec. IV C, are also apparent. For equal masses, the FFLO phase never meets the FP normal state. For mass ratios in excess of $r_c = (1+\sqrt{5})/2$, the FFLO phase meets the FP state on the majority "heavy" species side, but is further from the FP state on the "light" species side. For high mass ratios, this is evidenced by the much broader FFLO region on the heavy species side.

To conclude this section, it is interesting to compare the phase diagram of the ultracold atom system with contact interaction and the problem of electron-hole bilayers with long-ranged Coulomb interaction. In particular, we focus our discussion on the study in Ref. [50] of GaAs bilayers where the mass ratio $r=4.3$. In this case, it is more natural to characterize the strength of interaction by $r_s = r_0/a_0$, where $r_0 = 1/\sqrt{\pi n}$ denotes the interparticle spacing, and a_0 is the effective Bohr radius of the two-body bound state. The latter is

related to the dimensionless ratio E_b/E_F through the relation $E_b/E_F = 0.381 r_s^2$. As a result, we find that the system enters the BCS phase with the appearance of FFLO phase behavior for r_s values of around 1.5 (4) compared with that found for the unscreened electron-hole bilayer of $r_s \sim 1.5$ (16) for the "light" ("heavy") species. More qualitatively, in both cases, the systems show a preference toward the superfluid phase when the "light" species is in excess, and the normal phase when the "heavy" species is in excess. Although the topology of the phase diagram is quantitatively the same, two significant differences appear. The first is that, with the electron-hole bilayer, the FFLO-SF phase boundary on the "heavy" species side penetrates further into the BEC regime than in the ultracold atomic gas. The second difference is that, with the electron-hole bilayer, the FFLO region existed from the normal phase to $m=0$, and no phase separation between FFLO and SF was seen, except for the deep in the BEC regime. However in the ultracold atomic gas, phase separation of the SF was seen into a balanced SF and a FFLO phase. Both of these differences indicate that, with the electron-hole bilayer, the FFLO phase was more stable relative to the SF than in the ultracold atomic gas. This could be due to the long-range forces that act in the electron-hole bilayer whereas the ultracold atomic gas experiences only contact forces that would favor formation of tightly-bound BEC pairs.

V. HARMONICALLY TRAPPED SYSTEM

Finally, focusing on applications to ultracold atomic gases, we now address the influence of the trap geometry on the phase behavior. Here we make use of the local density approximation in which the chemical potential of both species $\mu_\sigma(\mathbf{R}) = \mu_\sigma - V(\mathbf{R})$ are renormalized by the same local trapping potential $V(\mathbf{R})$, the chemical potential difference h remains fixed across the trap. Moreover, we further assume that the spatial coordinates are rescaled to ensure a spherically symmetric trapping potential, $V(\mathbf{R}) = \omega R^2/2$. Although there is some experimental evidence [71,72] that the local density approximation might not be valid [15,73] in some setups, we believe that its application here will correctly address the qualitative phase structure.

To identify the phases present, one may consider a trajectory of changing μ with constant h and r in the phase diagram of fixed chemical potentials. To find the total magnetization and number of particles in the trap, one may make use of the local relations $m = -d\Omega/dh$ [Eq. (2)] and $n = -d\Omega/d\mu$ [Eq. (3)], respectively, and then integrate over the trap. All trajectories will end up, at large enough radius, in the ZP regime, which is the edge of the particle distribution.

The profiles in four sample traps are shown in Fig. 6, which follow trajectories highlighted in Fig. 4. The first three have species with equal masses $r=1$. At zero population imbalance only the SF state is observed. With a population imbalance, first there is a central balanced SF region surrounded by a ring of FP majority spin particles. On increasing the population imbalance yet further, between the ring of FP particles and the central SF, an FFLO instability adjacent to a PP region is seen. The first-order transition between the
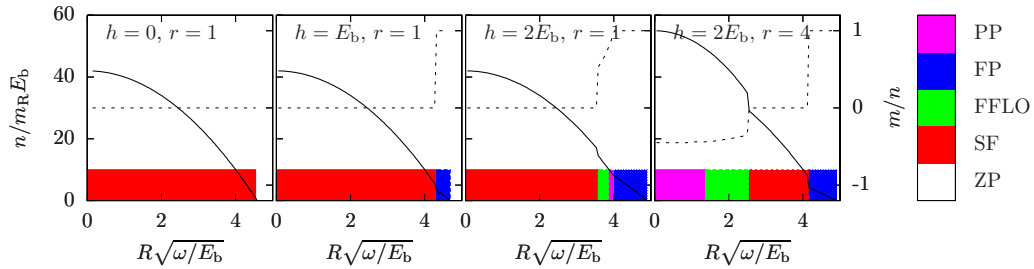
FIG. 6. (Color online) Radial density profiles of four systems in identical harmonic traps with different values of population imbalance h and mass ratio r. The solid line shows the radial density based on the primary y axis. The dashed line shows the local population imbalance based on the secondary y axis. The band shows where different phases exist with colors labeled on the right-hand side of the figure. With changing radial coordinate, the separate panels are associated with the trajectories highlighted in the $(h/E_b, \mu/E_b)$ phase diagram shown in Fig. 4.

SF and FFLO region (and FP state) leads to a discontinuity in density and polarization. The second-order transitions between FFLO, PP, and FP states have continuous variation of density and polarizability but discontinuous changes in their gradients.

The final profile in Fig. 6 is at an unequal mass ratio r =4. The inclusion of mass imbalance causes the SF region in Fig. 4 to be biased towards the "lighter" species. This means that it is possible to have a ring of superfluidity remote from the trap center, or an isolated ring of FFLO instability not at the center and no accompanying SF region. When there are two rings of normal phase bounding the SF they may either both be the "heavy" particle normal phase if we are crossing the extrusion of the FFLO phase, or alternatively one might be "light" and the other "heavy" if traversing right across the skewed SF phase. In the latter case, shown in Fig. 6, the species favored by the chemical potential shift dominates at the outside of the trap. At the center of the trap, the normal state is of the "heavy" species as superfluidity favors the "lighter" species.

VI. CONCLUSIONS

We have derived an analytic expression for the thermodynamic potential of a two-dimensional two-component atomic Fermi gas in the mean-field approximation with population imbalance and general mass ratio at zero temperature. A complementary Ginzburg-Landau analysis was used to ex-

amine the PP-FFLO transition. Analytical expressions for the phase boundaries separating normal and inhomogeneous superfluid phases have been obtained while the properties of the FFLO phase have been addressed numerically. Within the mean-field approximation, the SF phase does not sustain a population imbalance. The region of FFLO instability exhibits a second-order phase transition from the PP normal phase, and first-order phase transition into the balanced SF. In the BCS limit, a small population imbalance is sufficient to destroy pairing. In the BEC limit, there is phase separation between tightly bound molecules and a FP normal phase. If there is a mass imbalance, the SF phase is favored if the majority particles are the "lighter" species, while the polarized normal state is favored if the "heavy" species are in excess.

A trapped geometry leads to a rich range of possible density profiles. If there is no mass imbalance, a SF phase is seen at the trap center surrounded by a PP followed by a FP normal phase of the majority spin species. If there is mass imbalance, then a ring of the SF and/or the FFLO state could be seen bordered both inside and outside by either species of normal phase particles.

[1] C. A. Regal, M. Greiner, and D. S. Jin, Phys. Rev. Lett. **92**, 040403 (2004).

[2] M. W. Zwierlein, C. A. Stan, C. H. Schunck, S. M. F. Raupach, A. J. Kerman, and W. Ketterle, Phys. Rev. Lett. **92**, 120403 (2004).

[3] W. Ketterle and M. W. Zwierlein, e-print arXiv:0801.2500v1.

[4] T. Loftus, C. A. Regal, C. Ticknor, J. L. Bohn, and D. S. Jin, Phys. Rev. Lett. **88**, 173201 (2002).

[5] K. E. Strecker, G. B. Partridge, and R. G. Hulet, Phys. Rev. Lett. **91**, 080406 (2003).

[6] S. Gupta, M. W. Hadzibabic, Z. Zwierlein, C. A. Stan, K.

Dieckmann, C. H. Schunck, E. G. M. van Kempen, B. J. Verhaar, and W. Ketterle, Science **300**, 1723 (2003).

[7] C. Chin, M. Bartenstein, A. Altmeyer, S. Riedl, S. Jochim, J. Hecker, and G. R. Denschlag, Science **305**, 1128 (2004).

[8] M. Greiner, C. A. Regal, and D. S. Jin, Nature (London) **426**, 537 (2003).

[9] P. F. Bedaque, H. Caldas, and G. Rupak, Phys. Rev. Lett. **91**, 247002 (2003).

[10] A. Sedrakian, J. Mur-Petit, A. Polls, and H. Müther, Phys. Rev. A **72**, 013613 (2005).

[11] J. Kinnunen, L. M. Jensen, and P. Törmä, Phys. Rev. Lett. **96**,

110403 (2006).

[12] F. Chevy, Phys. Rev. Lett. **96**, 130401 (2006).

[13] P. Pieri and G. C. Strinati, Phys. Rev. Lett. **96**, 150404 (2006).

[14] C.-H. Pao, S.-T. Wu, and S.-K. Yip, Phys. Rev. B **73**, 132506 (2006).

[15] T. N. De Silva and E. J. Mueller, Phys. Rev. A **73**, 051602(R) (2006).

[16] J. Dukelsky, G. Ortiz, S. M. A. Rombouts, and K. Van Houcke, Phys. Rev. Lett. **96**, 180404 (2006).

[17] H. Hu and X.-J. Liu, Phys. Rev. A **73**, 051603(R) (2006).

[18] D. E. Sheehy and L. Radzihovsky, Phys. Rev. Lett. **96**, 060401 (2006).

[19] M. Haque and H. T. C. Stoof, Phys. Rev. A **74**, 011602(R) (2006).

[20] X.-J. Liu and H. Hui, Europhys. Lett. **75**, 364 (2006).

[21] K. Machida, T. Mizushima, and M. Ichioka, Phys. Rev. Lett. **97**, 120407 (2006).

[22] M. Iskin and C. A. R. Sá de Melo, Phys. Rev. Lett. **97**, 100404 (2006).

[23] J. Tempere, M. Wouters, and J. T. Devreese, Phys. Rev. B **75**, 184526 (2007).

[24] W. Zhang and L.-M. Duan, Phys. Rev. A **76**, 042710 (2007).

[25] C.-H. Pao, S.-T. Wu, and S.-K. Yip, Phys. Rev. A **76**, 053621 (2007).

[26] M. Rizzi, M. Polini, M. A. Cazalilla, M. R. Bakhtiari, M. P. Tosi, and R. Fazio, e-print arXiv:0712.3364v1.

[27] L. He and P. Zhuang, e-print arXiv:0801.3127v1.

[28] S. Inouye, J. Goldwin, M. L. Olsen, C. Ticknor, J. L. Bohn, and D. S. Jin, Phys. Rev. Lett. **93**, 183201 (2004).

[29] C. A. Stan, M. W. Zwierlein, C. H. Schunck, S. M. F. Raupach, and W. Ketterle, Phys. Rev. Lett. **93**, 143001 (2004).

[30] C. Ospelkaus, S. Ospelkaus, L. Humbert, P. Ernst, K. Sengstock, and K. Bongs, Phys. Rev. Lett. **97**, 120402 (2006).

[31] F. Ferlaino, C. D'Errico, G. Roati, M. Zaccanti, M. Inguscio, G. Modugno, and A. Simoni, Phys. Rev. A **73**, 040702(R) (2006).

[32] M. Zaccanti, C. D'Errico, F. Ferlaino, G. Roati, M. Inguscio, and G. Modugno, Phys. Rev. A **74**, 041605(R) (2006).

[33] T. Gottwald and P. G. J. van Dongen, Eur. Phys. J. B **61**, 277 (2008).

[34] E. Wille *et al.*, Phys. Rev. Lett. **100**, 053201 (2008).

[35] M. Iskin and C. A. R. Sá de Melo, Phys. Rev. A **77**, 013625 (2008).

[36] M. M. Parish, F. M. Marchetti, A. Lamacraft, and B. D. Simons, Nat. Phys. **3**, 124 (2007).

[37] W. V. Liu and F. Wilczek, Phys. Rev. Lett. **90**, 047002 (2003).

[38] T. Mizushima, K. Machida, and M. Ichioka, Phys. Rev. Lett. **94**, 060404 (2005).

[39] J. Carlson and S. Reddy, Phys. Rev. Lett. **95**, 060401 (2005).

[40] D. T. Son and M. A. Stephanov, e-print arXiv:050758 (2005).

[41] G. G. Batrouni, M. H. Huntley, V. G. Rousseau, and R. T. Scalettar, Phys. Rev. Lett. **100**, 116405 (2008).

[42] Y. Chen, Z. D. Wang, F. C. Zhang, and C. S. Ting, e-print arXiv:0710.5484v1.

[43] T. K. Koponen, T. Paananen, J.-P. Martikainen, M. R. Bakhtiari, and P. Törmä, e-print arXiv:0711.4065v2.

[44] P. Fulde and R. A. Ferrell, Phys. Rev. **135**, A550 (1964).

[45] A. I. Larkin and Y. N. Ovchinnikov, Sov. Phys. JETP **20**, 762 (1965).

[46] A. Bianchi, R. Movshovich, C. Capan, P. G. Pagliuso, and J. L. Sarrao, Phys. Rev. Lett. **91**, 187004 (2003).

[47] S.-T. Wu and S. Yip, Phys. Rev. A **67**, 053603 (2003).

[48] Y. Shin, M. W. Zwierlein, C. H. Schunck, A. Schirotzek, and W. Ketterle, Phys. Rev. Lett. **97**, 030401 (2006).

[49] X. Zhu, P. B. Littlewood, M. S. Hybertsen, and T. M. Rice, Phys. Rev. Lett. **74**, 1633 (1995).

[50] P. Pieri, D. Neilson, and G. C. Strinati, Phys. Rev. B **75**, 113301 (2007).

[51] T. Hakioğlu and M. Şahin, Phys. Rev. Lett. **98**, 166405 (2007).

[52] R. Combescot and C. Mora, Eur. Phys. J. B **44**, 189 (2005).

[53] B. P. Anderson and M. A. Kasevich, Science **282**, 1686 (1998).

[54] S. Burger, F. S. Cataliotti, C. Fort, F. Minardi, M. Inguscio, M. L. Chiofalo, and M. P. Tosi, Phys. Rev. Lett. **86**, 4447 (2001).

[55] F. S. Cataliotti, S. Burger, C. Fort, P. Maddaloni, F. Minardi, A. Trombettoni, A. Smerzi, and M. Inguscio, Science **293**, 843 (2001).

[56] J. K. Chin, D. E. Miller, Y. Liu, C. Stan, W. Setiawan, C. Sanner, K. Xu, and W. Ketterle, Nature (London) **443**, 961 (2006).

[57] J.-P. Martikainen and H. T. C. Stoof, Phys. Rev. A **68**, 013610 (2003).

[58] M. Wouters, J. Tempere, and J. T. Devreese, Phys. Rev. A **70**, 013616 (2004).

[59] W. Zhang, G.-D. Lin, and L.-M. Duan, e-print arXiv:0801.2500v1.

[60] J. A. Bowers and K. Rajagopal, Phys. Rev. D **66**, 065002 (2002).

[61] V. N. Efimov, Phys. Lett. **33B**, 563 (1970).

[62] V. N. Efimov, Nucl. Phys. A. **210**, 157 (1973).

[63] M. A. Baranov, C. Lobo, and G. V. Shlyapnikov, e-print arXiv:0801.1815v1.

[64] Q. Chen, J. Stajic, S. Tan, and K. Levin, Phys. Rep. **412**, 1 (2005).

[65] W. Yi and L. M. Duan, Phys. Rev. A **73**, 063607 (2006).

[66] J. Zhang and H. Zhai, Phys. Rev. A **72**, 041602(R) (2005).

[67] M. Randeria, J.-M. Duan, and L.-Y. Shieh, Phys. Rev. B **41**, 327 (1990).

[68] R. Casalbuoni and G. Nardulli, Rev. Mod. Phys. **76**, 263 (2004).

[69] H. Burkhardt and D. Rainer, Ann. Phys. **3**, 181 (1994).

[70] H. Shimahara, Phys. Rev. B **50**, 12760 (1994).

[71] G. B. Partridge, W. Li, R. I. Kamar, Y. Liao, and R. G. Hulet, Science **311**, 503 (2006).

[72] G. B. Partridge, W. Li, Y. A. Liao, R. G. Hulet, M. Haque, and H. T. C. Stoof, Phys. Rev. Lett. **97**, 190407 (2006b).

[73] A. Imambekov, C. J. Bolech, M. Lukin, and E. Demler, Phys. Rev. A **74**, 053626 (2006).